Phase Separation and Segregation Morphology of PCL/PS Blends: Quantitative Effect of the Crystallization Temperature, Composition, and Molecular Weight of PS

Leonel Ignacio Silva, Úrsula María Montoya Rojo, Carmen Cristina Riccardi
INTEMA, Facultad de Ingeniería, Universidad Nacional de Mar del Plata, Consejo Nacional de Investigaciones Científicas y Técnicas (CONICET), Av. Juan B. Justo 4302, Mar del Plata, 7600, Argentina

The phase diagrams for blends of semicrystalline poly(ε-caprolactone) (PCL) with amorphous polystyrene (PS) were determined and it was noticed that when molecular weight increases, the critical composition diminishes while its temperature increases. That is the same effect that produces the increase in the polydispersity of PS. From the fitting of phase diagrams of blends of PCL with oligomers and homopolymers of PS, taking into account the polydispersity, it was possible to conclude that the miscibility in these systems is due only by entropic effects. The crystalline fraction as well as the interlamellar spacing increased with crystallization temperature while the volume fraction of the amorphous PCL in the interfibrillar regions increases for the pure PCL and in its blends with low concentration of PS. Increasing the mass fraction of PS increases the average long spacing (*L*) till a weight fraction of 60%, for higher mass fractions *L* is almost constant indicating the interfibrillar segregation of PS. The PCL lamellar morphology is not affected when the molecular weight of PS employed is similar or higher than the molecular weight of PCL. If the PS has a higher molecular weight its penetration into the structure is inhibited. POLYM. ENG. SCI., 00:000–000, 2016.

INTRODUCTION

Polymer blends have gained much attention due to the potential for wide application in a variety of industries, government and academic training camps in recent decades [1, 2]. The main reason for the increasing development of polymer blends compared with the pure components is that the polymer blends have a variety of important features when they solidify [3, 4]. This depends on the supramolecular structure and phase morphology. In particular, blends containing semicrystalline polymer with amorphous polymer such as poly(ε-caprolactone) (PCL) with polystyrene (PS) are attractive materials because of its sustainability, respect for the environment, and their ability to form a wide range of materials [5, 6]. PCL is semicrystalline biodegradable polyester with a low melting point, which can be used for the preparation of blends with different polymers [7–10]; these properties make it a versatile material for theoretical and fundamental studies of blends. On the other hand, the general purpose PS is amorphous, clear, hard, and brittle and it is a low-cost polymer per unit weight.

Correspondence to: C. C. Riccardi; e-mail: criccard@fi.mdp.edu.ar
DOI 10.1002/pen.24480
Published online in Wiley Online Library (wileyonlinelibrary.com).

The blends of PCL with PS oligomers (PSO) present an upper critical solution temperature (UCST) phase diagram and the miscibility gap intersects the crystallization curve [3, 11–14]. Such type of diagram is shown qualitatively in Fig. 1.

Tanaka and Nishi [15] were the first to report the existence of coupling between crystallization and demixing in crystallizable blends with such kind of phase diagram. When the system is quenched from the isotropic region to a crystallization temperature, different morphologies can be developed due the competition between processes crystallization and phase separation depending on the composition [12]. Four important situations can be distinguished on Fig. 1:

Route 1: crystallization induced decomposition
Route 2: simultaneous bimodal decomposition and crystallization
Route 3: decomposition induced crystallization
Route 4: simultaneous spindle decomposition and crystallization

Routes 1 and 4 of Fig. 1 were discussed by Tanaka and Nishi [11, 13–15] for a system consisting of PCL and PS. In Case 1 the spherulites are separated and show large droplets on their surface, while in Case 4 coarse spherulite results including PS droplets. Li et al. [3] investigated Case 1 and 2 for the same system, that is, PCL/low molecular weight PS. For route 1 three different regimes can still be distinguished depending upon the rate of crystallization, v_C, and the rate of diffusion of the noncrystallizable component, v_D. If $v_D \ll v_C$, the noncrystallizable component is trapped within the growing crystals. Depending on the composition of the amorphous phase, liquid–liquid demixing may occur resulting in droplets of non-crystallizing polymer inside the spherulites. When $v_D \cong v_C$, a part of the amorphous component is trapped and another part is segregated from the growing crystals; the concentration of this component increases with crystallization and finally demixing occurs resulting in the formation of droplets at the spherulite surface. The third regime is presented if $v_D \gg v_C$ the noncrystalline component is fully segregated into the bulk melt and when the miscibility gap is reached the melt phase separates homogeneously and binodally. According to route 2, the crystallization starts from an already completely binodally demixed blend and the droplets, which are formed during demixing, are globular.

However, the architecture of spherulites is much more complex and requires more information than that given by a model of the lamellar structure alone. The crystallization implies the segregation of amorphous polymer chains and, depending on the distance of segregation, different types of morphology can coexist in the system; this includes: interlamellar (amorphous chains between lamellae), interfibrillar (amorphous chains between lamellar bundles or stacks of lamellae), and interspherulitic

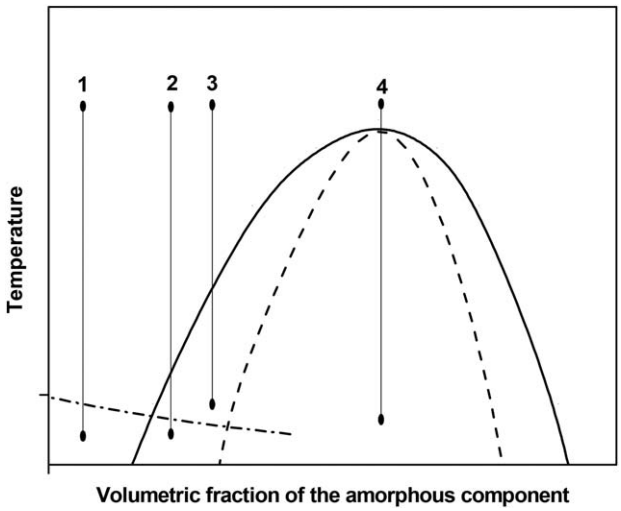

FIG. 1. Phase diagram of a PCL/PSO blend: binodal (solid line), spinodal (dash line), and crystal-melt coexistence curve (dash dot line).

(amorphous chains between spherulites) segregation [16]. The last case of segregation can be called intraspherulitic because one distinguishes of other two types and implies the creation of droplets of the amorphous almost pure component [17].

Most studies have focused on revealing the morphology in specific systems; nevertheless, there is a limited amount of researches that has evaluated the variables that could affect the segregation morphology. Talibuddin et al. studied the effect of intermolecular interaction and the glass transition temperature (T_g) of the diluent on the segregation distance [18]. They concluded that for weakly interacting systems, diluents T_g govern the length scale of segregation while the presence of strong interactions helps to promote segregation distance by depressing the crystal growth rate. On the other hand, the molecular weight of components is other variable because it may change the kinetic and thermodynamic parameters favoring the segregation distance. Chen et al. studied the effect of the molecular weight of PCL and PVC on the segregation morphology and they concluded that the factors that influence the growth rate are the factors that control the segregation distance and hence is expected that the crystallization temperature, T_c, may play an important role [19]. With respect to the latter subject Baldenegro Pérez et al. [20], studied the effects of T_c on the crystallization poly (ethylene terephthalate) homopolymers and defined three different morphological regions as a function of T_c. In low T_c region, crystallized samples were characterized by a low crystalline degree with a small spherulite texture containing thin crystals. In intermediate T_c region, samples showed medium size spherulites and the crystallization exhibited a maximum value and it was associated with a high content of secondary crystals. In high T_c range, samples presented considerable amorphous zones and regions consisting of oversized spherulites containing only thick crystals.

There are a few publications treating quantitatively the simultaneous effect of the crystallization temperature, composition, and the molecular weight of the amorphous component, since are variables that could affect the formation of segregation morphology; we do not know of such studies in bulk blends of PCL/PS.

The purpose of this study is to evaluate the influence of the number average molecular weight of the amorphous component (Mn_{PS}), its polydispersity and its weight fraction (w_{PS}), at different crystallization temperatures (T_c), on the segregation morphology in blends of PCL/PS. We will also evaluate the effect of T_c on the pure PCL morphology. With this aim phase diagrams for blends of PCL with PS of different molecular weight must be determined.

EXPERIMENTAL

Materials

Poly(ε-caprolactone) (PCL) was purchased to Aldrich Chemical Company (The United States), and polystyrenes (PS) were obtained from Polymer Source (Canada); their number average molecular weight (*Mn*) and dispersion index (*DI*) are shown in Table 1. Three series of PCL/PS blends, all of them with the same PCL, were studied. ***Series A*** are blends of PCL/PS_1 with different compositions (80/20; 60/40; 40/60 and 20/80), ***Series B*** are blends with different PS but all samples having the same mass relation (20/80), and ***Series C*** are blends of PCL/PS_5 with different compositions (80/20; 60/40; 40/60; and 20/80).

Sample Preparation

The blends were prepared by dissolving the polymer in chloroform [21, 22]. The polymer concentration in the solution was 5% by weight and the solution was carried out by magnetic stirring at 40°C and 350 rpm until complete solubility. To optimize the process, the samples were sonicated at the same temperature over a period of 5 min. Evaporation of solvent was carried out at room temperature using a Petri dish, until constant weight was reached. Before performing any of the measures samples were carried to a high enough temperature, that depends of the blend, for their homogenization; then, they were rapidly cooled to avoid crystallization (cooling rate ~60°C/min) to the desired crystallization temperature (T_c), and finally kept at T_c for 4 h to induce the crystallization process.

Small Angle X-Ray Scattering Diffraction (SAXS)

SAXS measurements were performed at the Brazilian Synchrotron Light Laboratory (LNLS) CNPEM/MCT, line SAXS1 in Campinas, Brazil. A wavelength of $\lambda = 1.49$ Å was selected for the monochromatic beam used in the experiments. The low-angle scatter was registered to the scattering vector q ($q = (4\pi/\lambda)\ \sin\alpha$), where 2α is the scattering angle, between $q_{min} = 0.1\ nm^{-1}$ and $q_{max} = 0.3\ nm^{-1}$ using a position sensitive detector for the small-angle region located at a distance of 1.216 m from the sample. The 2D scattering profiles were radially averaged and converted to 1D data using the program

TABLE 1. Homopolymers used in studied blends.

Polymer	*Mn* (g/mol)	DI
PCL	10,000	1.4
PS_1	3,700	1.1
PS_2	1,400	1.1
PS_3	3,700	1.2
PS_4	10,400	1.1
PS_5	85,000	1.3

DOI 10.1002/pen

FIT2D V12.077. Dispersion curves of experimental small angle were normalized with the integrated intensity of the beam incident. Various tests were carried out in order to ensure the repeatability of measurements. The samples for SAXS experiments were crystallized at 30°C and 40°C. These T_c were selected because the PCL used in this study has an optimal crystallization temperature, defined as T_c at which the Avrami exponent is 3 [20], 42° C (experimental results not shown in this article).

Differential Scanning Calorimetry (DSC)

DSC measurements of pure PCL and PCL/PS blends were performed on Shimadzu DSC-50 equipment. Samples of approximately 10 mg were encapsulated in aluminum pans and measured under nitrogen atmosphere. Temperature and heat of fusion were calibrated by using pure indium metal as a standard reference. The melt/PCL-crystal coexistence curve or equilibrium melting temperature versus the mass fraction of PS was determined by relating the isothermal crystallization, T_c, and melting, T_m, temperatures of samples with different composition and extrapolating their relation to $T_c = T_m$ (Hoffman–Weeks-plot [23]).

Microscopy

A Leica DM LB optical microscope (OM) with a Linkam THMS 600 hot stage was used for the essays. To determine cloud-points temperatures, T_{cp}, of blends containing different concentrations, the temperature was increased until a homogeneous solution is obtained, kept constant during several minutes and then decreased at a cooling rate in the order of 1 K/min. The T_{cp} value is determined at the onset time of the light transmission decrease.

Confocal Raman microscopy (CRM) InVia Reflex objective 50× (NA: 0.75, 370 μm working distance) was used at room temperature to observed the morphology of the blends.

RESULTS AND DISCUSSION

Phase Diagrams

Theoretical Background. The phase diagram of an amorphous with a semicrystalline polymer is composed by (i) the cloud point curve, that represents the liquid–liquid equilibrium, and (ii) the crystal-melt coexistence curve, that represents the liquid–solid equilibrium.

The cloud point curve. Different approaches exist to model cloud points curve of blends and are described in a previous article [24]. We decided to calculate the cloud point curves from the Flory Huggins (FH) [25] energy equation following the procedure developed by Kamide et al. [26], where the polydispersities of both blend components are considered. The polymers are assumed to have a continuous molar mass distribution obtained using the Schulz–Zimm equation [27]:

$$w_i = \frac{g^{hr+1}}{\Gamma(hr+1)}\, i^{hr} \exp(-g\, i) \tag{1}$$

with

$$hr = \frac{\overline{Z_w}}{\overline{Z_n}} - 1 \text{ and } g = \frac{hr}{\overline{Z_n}} \tag{2}$$

In the above expressions w_i is mass fraction of macromolecules with a polymerization degree i, Γ is the gamma function, while $\overline{Z_n}$ and $\overline{Z_w}$ are number and weight size averages, respectively.

For a fluid mixture of two polydisperse polymers, with volume fractions given by:

$$\varphi_1 = \sum_i \varphi_i = \varphi_1^0 \sum_i w_i \text{ and } \varphi_2 = \sum_j \varphi_j = \varphi_2^0 \sum_j w_j \tag{3}$$

and the FH equation written in terms of Gibb free energy of mixing per mol of unit cells, ΔG, is given by:

$$\frac{\Delta G}{RT} = \frac{1}{Z_1}\sum_i \frac{\varphi_i}{i} \ln\varphi_i + \frac{1}{Z_2}\sum_j \frac{\varphi_j}{j} \ln\phi_j + \chi(T)\varphi_1\varphi_2 \tag{4}$$

where χ is the temperature dependent interaction parameter, R is the gas constant, T is the absolute temperature (K), φ_1 and φ_2 are volume fractions of species 1 (PCL) and 2 (PS) and Z_1 and Z_2 are the size of the homopolymers calculated as the ratio between the molar volume and the reference volume that was taken as the smallest species volume.

The chemical potentials μ_i and μ_j can be obtained from Eq. *4* by the usual procedures:

$$\frac{\Delta\mu_i}{RT} = \left(\frac{\partial(\Delta G/RT)}{\partial n_i}\right)_{T,P,n\neq i} \text{ and } \frac{\Delta\mu_j}{RT} = \left(\frac{\partial(\Delta G/RT)}{\partial n_j}\right)_{T,P,n\neq j} \tag{5}$$

with n_i the specie mole number

$$\begin{aligned} \frac{\Delta\mu_i}{RT} &= 1 + \ln\varphi_i - Z_i\left[\left(\sum_i \frac{\varphi_i}{Z_i} + \sum_j \frac{\varphi_j}{Z_j}\right) + \chi\varphi_2^2\right] \text{ and} \\ \frac{\Delta\mu_j}{RT} &= 1 + \ln\varphi_j - Z_j\left[\left(\sum_i \frac{\varphi_i}{Z_i} + \sum_j \frac{\varphi_j}{Z_j}\right) + \chi\varphi_1^2\right] \end{aligned} \tag{6}$$

At the cloud point, there are two phases in equilibrium, α and β, and the well-known Gibbs law applies:

$$\Delta\mu_i^\alpha = \Delta\mu_i^\beta \text{ and } \Delta\mu_j^\alpha = \Delta\mu_j^\beta \tag{7}$$

By working with these equalities the following equations are obtained

$$\sigma_1 = \frac{1}{Z_i}\ln\frac{\varphi_i^\beta}{\varphi_i^\alpha} = \left(\sum_i \frac{\varphi_i^\beta}{Z_i} + \sum_j \frac{\varphi_j^\beta}{Z_j}\right) - \left(\sum_i \frac{\varphi_i^\alpha}{Z_i} + \sum_j \frac{\varphi_j^\alpha}{Z_j}\right) + \chi\left(\varphi_2^{\alpha^2} - \varphi_2^{\beta^2}\right) \tag{8}$$

and

$$\sigma_2 = \frac{1}{Z_j}\ln\frac{\varphi_j^\beta}{\varphi_j^\alpha} = \left(\sum_i \frac{\varphi_i^\beta}{Z_i} + \sum_j \frac{\varphi_j^\beta}{Z_j}\right) - \left(\sum_i \frac{\varphi_i^\alpha}{Z_i} + \sum_j \frac{\varphi_j^\alpha}{Z_j}\right) + \chi\left(\varphi_1^{\alpha^2} - \varphi_1^{\beta^2}\right) \tag{9}$$

where σ_1 y σ_2 are the separation factors such that

$$\varphi_i^\beta = \varphi_i^\alpha \exp(\sigma_1 Z_i) \text{ and } \varphi_j^\beta = \varphi_j^\alpha \exp(\sigma_2 Z_j) \tag{10}$$

TABLE 2. Homopolymers used in the construction of published diagrams.

	PCL		PS	
Reference	*Mn* (g/mol)	DI	*Mn* (g/mol)	DI
Li et al. [2]	10,000	1.50	765	1.10
Tanaka and Nishi [8]	10,700	3.08	840	1.13
Nojima et al. [9]	9,514	1.44	840	1.13

Considering that, at the beginning of the phase separation process $\varphi_1^{\alpha}=\varphi_1^0$ and $\varphi_2^{\alpha}=\varphi_2^0$ (initial composition) and the composition of the β-phase fulfills the balance:

$$\varphi_1^{\beta}+\varphi_2^{\beta}=1 \tag{11}$$

By introducing Eq. *10* in *Eqs. 8, 9,* and *11* we obtain a system of three non-linear equations with three unknowns σ_1, σ_2, and χ.

The rigorous expressions for spinodal and critical points, considering the polydispersity of polymers, were derived by Koningsveld and Staverman [28]:

Spinodal curve:

$$\frac{1}{\overline{Z_{1w}}\,\varphi_{1,s}}+\frac{1}{\overline{Z_{2w}}\,\phi_{2,s}}-2\,\chi=0 \tag{12}$$

Critical point condition:

$$\frac{\overline{Z_{1z}}}{\left(\overline{Z_{1w}}\,\varphi_{1c}\right)^2}+\frac{\overline{Z_{2z}}}{\left(\overline{Z_{2w}}\,\varphi_{2c}\right)^2}=0 \tag{13}$$

Critical composition:

$$\varphi_{1,c}=\frac{\left(\overline{Z_{2w}}/\left(\overline{Z_{2z}}\right)^{0.5}\right)}{\left(\overline{Z_{1w}}/\left(\overline{Z_{1z}}\right)^{0.5}\right)+\left(\overline{Z_{2w}}/\left(\overline{Z_{2z}}\right)^{0.5}\right)}\ \text{and}\ \varphi_{2,c}=1-\varphi_{1,c} \tag{14}$$

Critical interaction parameter:

$$\chi_c=\frac{1}{2}\left(\overline{Z_{1z}}^{0.5}+\overline{Z_{2z}}^{0.5}\right)\left(\frac{1}{\overline{Z_{2w}}\,\overline{Z_{1z}}^{0.5}}+\frac{1}{\overline{Z_{1w}}\,\overline{Z_{2z}}^{0.5}}\right) \tag{15}$$

where $\overline{Z_{1z}}$ and $\overline{Z_{2z}}$ are the size averages of polymers 1 and 2, respectively

The crystal-melt coexistence curve. Study of the melting point depression of the crystallizable component in a binary polymer blend can lead to an assessment of the Flory–Huggins interaction parameter χ between the blend components. This parameter results from the condition that the chemical potential of the polymer be identical in the melt and in the pure crystalline state. One can evaluate χ from the equilibrium melting points Tm^0 (mixture) and Tm_0^0 (pure substance) according to the Flory–Huggins theory modified by Nishi–Wang [29]

$$\frac{1}{Tm^0}-\frac{1}{Tm_0^0}=-\frac{R}{\Delta H_{1u}}\frac{V_{u2}}{V_{u1}}\left(\frac{\ln\varphi_1}{Z_1}+\varphi_2\left(\frac{1}{Z_1}-\frac{1}{Z_2}\right)+\chi\varphi_2^2\right) \tag{16}$$

where the subscript 1 represents the crystallizable polymer (PCL) and the subscript 2 stands for the component, which does not crystallize within the temperature range of interest (PS). V_{u1} and V_{u2} are the corresponding molar volumes of the repeating unit while ΔH_{1u} signifies the heat of fusion of PCL per monomeric unit and is equal to 15.5 kJ/mol [30].

TABLE 3. Experimental cloud point temperatures.

	T_{cp} (°C)		
w_{PS}	PS_1	PS_3	PS_4
0.30			170.5
0.40	110.9	127.0	190.0
0.50	107.8	132.9	197.0
0.55			203.5
0.60	122.2	130.1	204.5
0.70	120.2	132.0	216.0
0.80	119.8	130.0	225.0

Analysis of Experimental Results. To have the complete picture of binodal curves for blends of PCL with PS, we will fit both experimental results obtained for mixtures of PCL with PS1, PS3 and PS4 (blends of PCL with PS5 are totally immiscible) as those published results for PSO [3, 11–13]. The molecular weight characterization of the homopolymers used in published diagrams is shown in Table 2 while experimental cloud point temperatures, $T_{CP,}$ are shown in Table 3.

By solving the system of Eqs. *8*, *10*, and *11*, χ parameters were obtained and they were correlated with the temperature as shown in Fig. 2.

In Fig. 2 experimental points can be fitted by two lines that show the UCST behavior of these blends. For the blends of PCL with PSO is:

$$\chi=0.0517+\frac{18.195}{T(K)} \tag{17}$$

This value is very close to that reported by Li et al. [3] that was calculated without taking into account the polydispersity. The corresponding expression of χ for the blends of PCL with PS of higher molecular weight is:

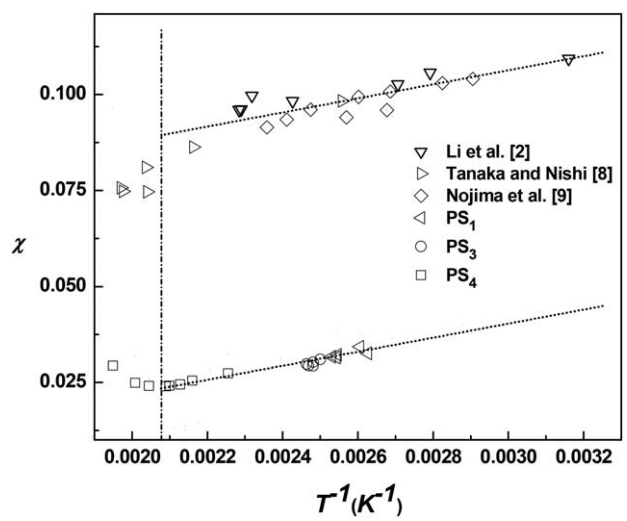

FIG. 2. Interaction parameter.

DOI 10.1002/pen

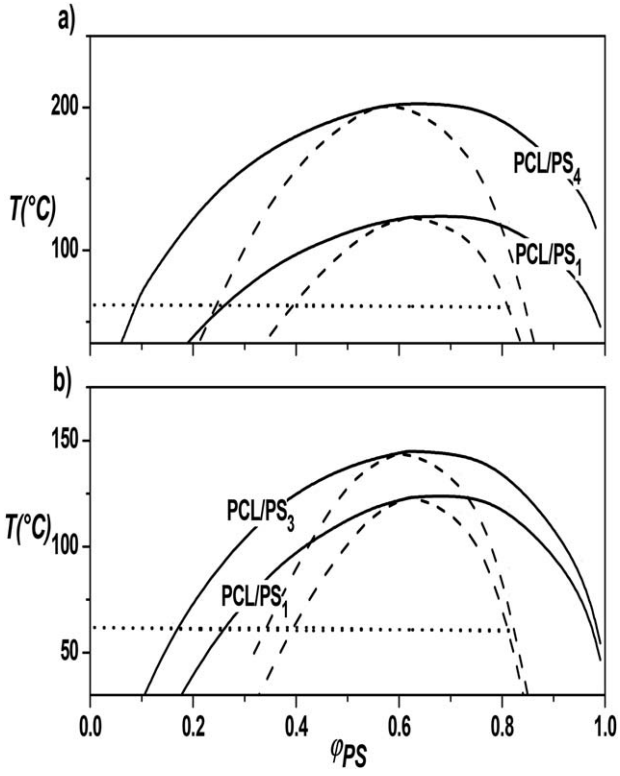

FIG. 3. Phase diagrams of PCL/PS blends.

$$\chi = -0.0143 + \frac{18.186}{T(K)} \tag{18}$$

By comparing the expressions given by Eqs. *17* and *18* it is possible conclude that both χ has the same enthalpic contribution but the entropic ones diminishes for the PS homopolymers [31].This same effect was observed when were studied the UCST behavior of blends of polyetherimide with epoxy prepolymers of the type of diglycidyl ether of bisphenol A with different molecular weight [32]. This indicates that there are only slight repulsory energetic interactions between the components and that the miscibility in these systems is due only by entropic effects.

For high temperatures, to the left of the dotted line in Fig. 2 ($T_{cp} > 210$°C), the fitting is not so good probably due to the high weight average molecular weight of PCL used by Tanaka and Nishi or the high number average molecular weight of PS_4 that can produce some thermal degradation.

Spinodal curves were calculated with *Eq. 12*. The predicted binodal and spinodal curves and experimental Tm^0 values are shown in Fig. 3. In the Fig. 3a the blends PCL/PS_1 and PCL/PS_4 are compared: when Mn_{PS} increases, the critical composition diminishes while its temperature increases. The effect that produces the increase of the polydispersity on the phase diagram is the same that took place on having increased Mn_{PS} as it appears in the Fig. 3b, where there are compared results for the blends PCL/PS_1 and PCL/PS_3.

The composition and the χ parameter of the critical point, χ_{crit}, are shown in Table 4. The values of $\varphi_{PS,crit}$ predicted for the blends with PSO are coincident with those determined experimentally in cited works. As PCL homopolymers used in this blends have more or less the same molecular weight than that used in this study it is possible to examine the effect of the molecular weight of PS homopolymers: as it is expected the $\varphi_{PS,crit}$ tends to 0.5 as the average sizes of the homopolymers in the mixture are equalize. The effect of the polydispersity of PCL on the phase diagram can be explained by comparing the parameters of the critical point of the works published for PCL/PSO blends (see Table 4), ignoring the little difference in molecular weights of the homopolymers: the highest polydispersity implies the highest $\varphi_{PS,crit}$ and the lesser χ_{crit}, fact that can be translate in a highest critical temperature.

The determined value of Tm_0^0 of pure PCL is equal to 61.8°C in accord with published results by Huang et al. [33].The melting point depression is only slight and amounts are in the range of -0.017 to -0.033 K/w_{PS} for all the blends studied, in accord with that determined by Li et al. [3].

Matkar and Kyu [34] modelize the system described by Tanaka and Nishi [11] expressing the total free-energy density of mixing of the crystal-amorphous polymer blend as the weighted sum of the free-energy density pertaining to crystal order parameter [35] of the crystalline constituent with its volume fraction and the free energy of liquid-liquid mixing as described by the Flory–Huggin's theory of mixing but do not include the polydispersity in the analysis. They determined two interaction parameters that are constants with temperature: the amorphous-amorphous interaction parameter at 60°C, $\chi_{aa} = 1.04$, and the crystal-amorphous interaction parameter, $\chi_{ca} = 0.44$. These values are not comparable with our results because they used the molar volume of the PS with a molecular weight of 950 g/mol as reference volume that is 9.135 times our reference volume. With this in mind the corrected values are: $\chi_{aa} = 0.114$ and $\chi_{ca} = 0.048$. The value of χ_{aa} coincides with our value at 60°C (see Fig. 2).

From the χ versus φ_{PS} curve (not shown here) we determined the χ_{ca} value at the φ_{PS} were both curves intercept, and we compared experimental Tm^0 with those arising from *Eq. 16*. Results are shown in Table 5. The χ_{aa} parameter is in the order of that determined by Matkar and Kyu [34] and there is a good agreement between experimental and predicted temperatures.

Segregation Morphologies

In order to obtain information about the lamellar morphology of the samples, results obtained by SAXS for pure PCL and PCL/PS_1 blends are presented in terms of $I(q)\ q^2$ versus q (Lorentz representation), where I is the scattering intensity of each sample [36]. After extrapolating the intensity to smaller and larger angles by Guinier's and Porod's laws, respectively, the one-dimensional correlation function $\gamma(r)$ was evaluated using *Eq. 17* [37]:

TABLE 4. Composition and interaction parameter of the critical point.

Reference	$\phi_{PS,crit}$	χ_{crit}
Li et al [2]	0.784	0.096
Tanaka and Nishi [8]	0.821	0.076
Nojima et al. [9]	0.770	0.089
PS_1/PCL	0.620	0.032
PS_3/PCL	0.618	0.029
PS_4/PCL	0.564	0.024

TABLE 5. Predicted temperature of the intersection point between curves of cloud point and crystal-melt coexistence.

			Tm^0(°C)	
	χ_{aa}	ϕ_{PS}	Experimental	Predicted
PS_1	0.0405	0.2602	61.30	61.50
PS_3	0.0408	0.1695	61.29	61.50
PS_4	0.0399	0.0893	61.60	61.70

$$\gamma(r)=\frac{\int_0^\infty q^2 I(q)\cos(qr)dq}{\int_0^\infty q^2 I(q)dq} \tag{17}$$

As an example, the panel a in Fig. 4 shows the Lorentz representation for blend PCL/PS_1 80/20, belonging to ***Series A,*** crystallized at 30°C. The observed maximum in the curve is associated with the average long period (L) between the centers of adjacent lamellae [38–40]. In the insert of Fig. 4 (panel b), the one-dimensional correlation function (γ) is represented as a function of the distance, r. In order to obtain information about the main distances in a semicrystalline polymer the follow procedure was used to obtain L, and the thickness of each phase l_1 and $l_2 = L - l_1$ [36].

In a perfect lamellar structure it is assumed that L is equal to the sum of to the thickness of the amorphous (l_a) or crystalline (l_c) regimens [37] but there is an inherent problem with the interpretation of the information obtained from SAXS originated from the principle of Babinet [36] and in some cases, leads to an ambiguity in the allocation of the two main distances of a semi-crystalline structure. Then considering that parameters l_1 and l_2 can represent l_a or l_c (depending on the sample) and that l_c/L is the linear degree of crystallinity within the lamellar stacks, Φ_l, the assignment of these parameters has to be done with the help of the bulk degree of crystallinity of the blends, Φ_c, calculated from DSC measurements[16, 41].

According to results published by Plivelic *et al*. [16] one of the ratios l_i/L ($i = 1, 2$) obtained for SAXS is bigger and the

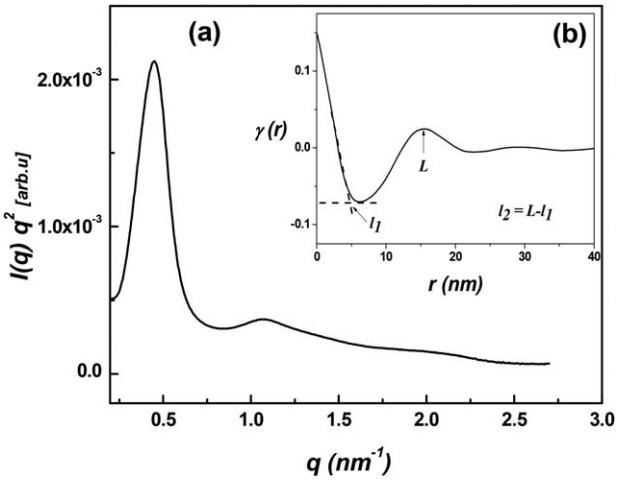

FIG. 4. **(a)** Lorentz-corrected SAXS profile for the blend PCL/PS_1 80/20, crystallized at 30°C. **(b)** Schematic presentation of a 1D correlation function $\gamma(r)$ and the morphological parameters obtained: L, l_1, and l_2.

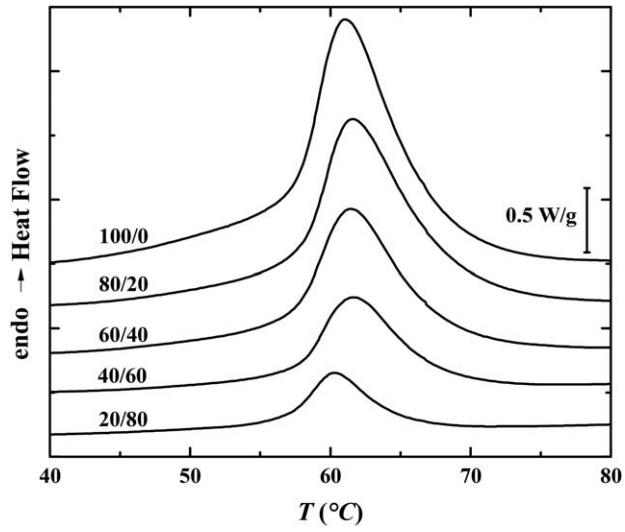

FIG. 5. Thermograms for pure PCL and its blends with PS_1, obtained after isothermal crystallization at 30°C.

other one smaller than Φ_c. As not all of the morphology in the blend is lamellar because depending of the localization of amorphous phase different morphologies can coexist (interlamellar, interfibrillar, and inter-spherulitic) [42], Φ_l is always bigger than or equal to Φ_c and the assignment of l_1 and l_2 as l_c or l_a can be done. Φ_c is defined as follows [42]:

$$\Phi_c=\frac{X_c/\rho_c}{\frac{X_c}{\rho_c}+\frac{w_{PCL}-X_c}{\rho_a}+\frac{1-w_{PCL}}{\rho_{PS}}} \tag{18}$$

where ρ_c and ρ_a are the densities of 100% crystalline and amorphous of PCL ($\rho_c = 1.187$ g/cm^3, $\rho_a = 1.094$ g/cm^3) [43] and ρ_{PS} is the density of PS ($\rho_{PS} = 1.05$ g/cm^3) [19]. X_c is the crystallinity of the blend defined by:

$$X_c=\frac{\Delta H_m}{\Delta H_m^0} \tag{19}$$

where ΔH_m is the heat of fusion of the samples obtained from the area under the curve of DSC thermograms (see Fig. 5), and ΔH_m^0 is the heat of fusion for a completely crystalline PCL, which has a value of 136 J/g according to the literature [44]. The crystalline fraction of PCL was calculated using:

$$X_{c,PCL}=\frac{X_c}{w_{PCL}} \tag{20}$$

TABLE 6. l_i/L ($i = 1,2$) obtained from the SAXS analysis of $\gamma(r)$ and Φ_c obtained from the measurement of ΔH_m by DSC for pure PCL and blends PCL/PS_1 for both isothermal crystallization temperatures studied.

	T_c = 30°C			T_c = 40°C		
w_{PS1}	l_1/L	l_2/L	Φ_c	l_1/L	l_2/L	Φ_c
0.0	33.1	66.9	48.6	26.5	73.5	55.0
0.2	34.0	65.7	36.7	31.4	68.6	39.9
0.4	–	–	26.6	32.5	67.5	34.0
0.6	40.5	59.4	17.1	33.8	66.2	18.8
0.8	41.1	58.9	7.8	36.5	63.5	11.8

DOI 10.1002/pen

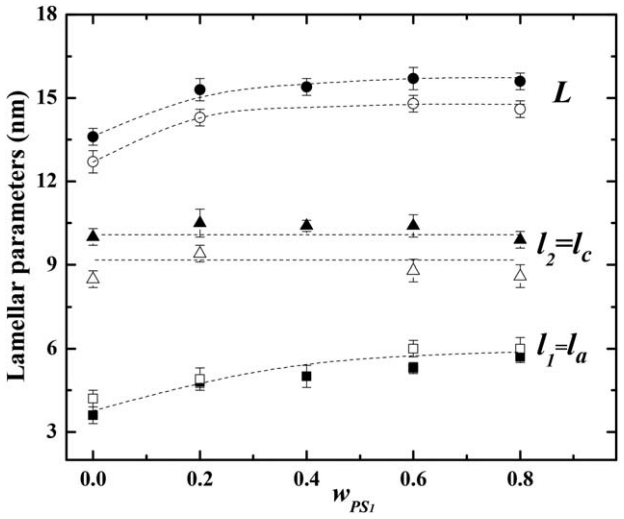

FIG. 6. Interlamellar spacing L, crystalline layer thickness l_c and amorphous layer thickness l_a for samples crystallized at 30°C (open symbols) and 40°C (filled symbols) as a function of PS content in blends of ***Series A***. Dash–dot lines are only an eye guide.

The parameters l_i/L $(i = 1,2)$ obtained from the analysis of $\gamma(r)$ for blends PCL/PS_1 studied at two crystallization temperatures 30°C and 40°C, respectively, together with Φ_c values obtained from DSC measurements, are presented in Table 6. For blends with w_{PS1} equal to 0.2 and 0.4, ratios, l_1/L and l_2/L are greater than Φ_c; in this case, the assignment was performed by considering the monotonic behavior of l_c. It is worth mentioning that bearing in mind the above discussion and the results shown in Table 6, it was concluded that l_2 corresponds to l_c while l_1 corresponds to l_a. Figure 6 shows the variation of the average long period L, crystalline layer thickness l_c and amorphous layer thickness l_a as a function of the weight fraction of PS_1 in the blends with the crystallization temperature as parameter. It is observed that while l_a is not affected by the heat treatment, l_c and L increase when T_c does. This observation suggests that the increase of the size of the lamellae is dependent on the temperature, although the temperature difference is only 10°C. This fact may be due to that the highest crystallization temperature approaches to the optimum one. For instance for pure PCL, L values are 12.7 ± 0.4 nm and 13.6 ± 0.3 nm, and l_c values are 8.5 ± 0.3 nm and 10 ± 0.3 nm for the temperatures studied ($T_c = 30$°C and 40°C, respectively). In blends l_c values, almost constant for all compositions, are 8.8 ± 0.4 nm at $T_c = 30$°C and 10.2 ± 0.3 nm $T_c = 40$°C. The average lamellar parameters of PCL observed are consistent with those obtained by Nojima et al. [45].

Furthermore, l_a and L increase with increasing the w_{PS1} in the blends, until they reach approximately constant quantities for values of w_{PS1} greater than 60% that corresponds to the critical point (see Table 4). This fact is indication of the interfibrillar segregation because PS molecules of the PS-rich phase can diffuse over large distances during the lamellar growth process of PCL. This long range diffusion results in an interfibrillar as well as interspherulitic segregation of the amorphous polymers at low PCL concentration [17, 46]. The behavior of l_c, l_a, and L as a function of PS content in the blend is similar to that reported by Nojima et al. in blends of PCL with PSO that has [13, 45]. Guo et al. [47] found in epoxy/PCL blends that epoxy molecules can be introduced between the lamellae of the crystalline polymer, increasing the characteristic dimensions of this region.

Linear crystallinity, Φ_l was used to quantify the interfibrillar morphology. It was related to the bulk crystallinity by [19]:

$$\Phi_c = \Phi_l \theta \tag{21}$$

where θ is the volume fraction of lamellar stacks in the sample. When $\theta = 1$, $\Phi_l = \Phi_c$ and whole volume is filled with lamellar stacks but if samples are not homogeneously filled with lamellar stacks implies that $\theta < 1$ and $\Phi_l > \Phi_c$. Moreover, PCL short chains also contribute to the interfibrillar morphology, so θ cannot be used directly for presenting the extent of amorphous segregation. θ is shown in Fig. 7a and defined as follows:

$$\theta = 1 - \theta_{PCL}^{a,IF} - \theta_{PS}^{IF} \tag{22}$$

In this expression, $\theta_{PCL}^{a,IF}$ is the volume fraction of the amorphous PCL short chains and θ_{PS}^{IF} is the volume fraction of PS both of them in the interfibrillar regions. Considering that all the PCL amorphous molecules that were non crystallizable after blending were expelled to the interfibrillar regions, $\theta_{PCL}^{a,IF}$ is then

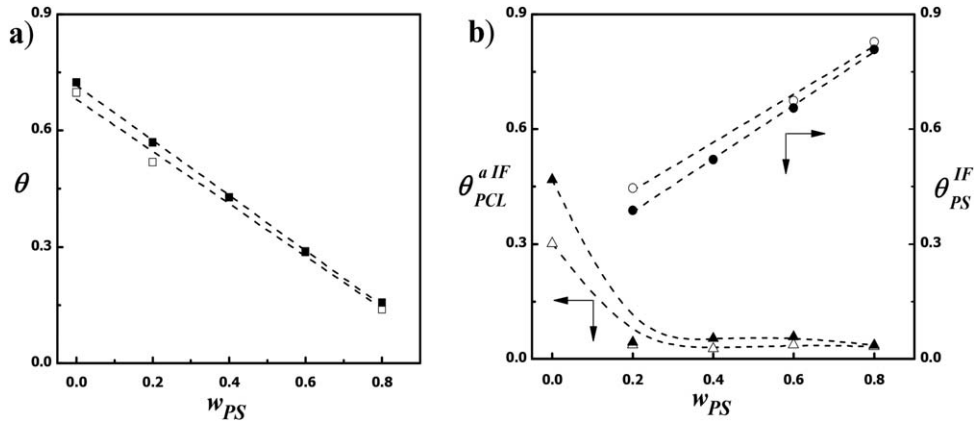

FIG. 7. Change of the volume fraction of (a) lamellar stacks (θ) and (b) of PS (θ_{PS}^{IF}) and PCL ($\theta_{PCL}^{a,IF}$) segregated interfibrillary with the mass fraction of PS in the blend for samples crystallized at 30°C (open symbols) and 40°C (filled symbols).

TABLE 7. Crystalline fractions of blends (X_c) and PCL ($X_{c,PCL}$), for pure PCL and PCL/PS_1 blends, crystallized at different temperatures (30°C and 40°C).

	$T_c = 30$°C		$T_c = 40$°C	
w_{PS1}	$X_c(\%)$	$X_{c,PCL}(\%)$	$X_c(\%)$	$X_{c,PCL}(\%)$
0.0	46.7	46.7	53.2	53.2
0.2	34.4	43.0	39.0	48.8
0.4	26.4	44.0	28.8	47.9
0.6	17.2	43.0	19.0	47.4
0.8	8.7	43.4	9.9	49.6

given by the difference in crystallizability between pure PCL and PCL in the blends with the same *Mn*, namely

$$\theta_{PCL}^{a,IF} = \left(w_c^0 w_{PCL} - w_c\right)\left(\frac{\rho}{\rho_{PCL}^a}\right) \quad (23)$$

where w_C^0 and w_c are the weight crystallinities of pure PCL and blend, respectively, and ρ and ρ_{PCL}^a are the densities of blend and amorphous PCL, respectively. $\theta_{PCL}^{a,IF}$ is then known and the volume fraction of PS expelled into the interfibrillar regions may be calculated with *Eq. 23* [19].

In Fig. 7a was observed that θ drops monotonically with w_{PS}; it is due to increased interfibrillar morphology indicating that the short chains of PS_1 were segregated interfibrillarly into the spherulite, also at lower T_c. As T_c decrease, the degree of the undercooling become bigger too growth rate increases as result, diffusion is less than the crystallization growths and the amorphous polymer can be trapped in the interfibrillar region. Values higher for $\theta_{PS}^{a,IF}$ shown in Fig. 7b were increasing with content of PS. While, the high crystallization temperature affects θ_{PS}^{IF} mostly in blends with low w_{PS} by the increased of interfibrillar segregation, other compositions show not significant changes due to crystallization temperature. T_c affected $\theta_{PCL}^{a,IF}$ in pure PCL, while in the blends, $\theta_{PCL}^{a,IF}$ not was affected significantly by w_{PS} or T_c.

In Table 7 are presented the crystalline fraction in the blends, X_c and the crystalline fraction of the PCL ($X_{c,PCL}$) for blends in the ***Series A*** at the crystallization temperatures studied. Values of X_c for the blends are lower than those of pure PCL, decreasing until approximately 80% in the range of blends studied due to the dilution effect of PS_1. It can be conclude that crystalline fraction remains constant for PCL as well as l_c, independently of the weight fraction of PS_1 in the blends. Similar situation was observed by Nojima et al. for PCL/PSO blends crystallized at 25°C, 34°C, and 45°C [13].

TABLE 8. *L* and $X_{c,PCL}$ for blends *(Series B)* crystallized at temperatures of 30°C and 40°C.

	$T_c = 30$°C		$T_c = 40$°C	
Series B	*L* (nm)	$X_{c,PCL}(\%)$	*L* (nm)	$X_{c,PCL}(\%)$
PCL/PS_1	14.6 ± 0.4	46.7	15.6 ± 0.3	53.2
PCL/PS_2	15.9 ± 0.4	46.6	17.3 ± 0.2	52.9
PCL/PS_3	14.0 ± 0.3	49.4	14.9 ± 0.4	54.3
PCL/PS_4	12.9 ± 0.3	47.8	13.2 ± 0.5	53.4
PCL/PS_5	12.8 ± 0.4	47.9	13.6 ± 0.4	53.5

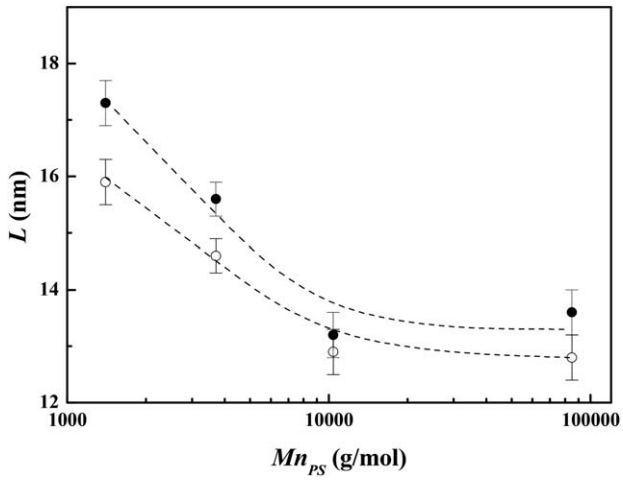

FIG. 8. Lamellar thickness (*L)* as a function of Mn_{PS} for samples crystallized at 30°C (open symbols) and 40°C (filled symbols).

In Table 8 are presented *L* and $X_{c,PCL}(\%)$ for the different blends PCL/PS (20/80) corresponding to the ***Series B*** at both crystallization temperature studied. While the sample of the blend PCL/PS_5 is totally immiscible, the composition of other blends is richer in PS than that of the critical point. For the blends of this Series, the value of *L* decreases with an increase in Mn_{PS} at both crystallization temperatures studied. Remembering pure PCL values of *L* (12.7 ± 0.4 nm and 13.6 ± 0.3nm, $T_c = 30$°C and 40°C, respectively), the increase of *L* becomes more evident for PS_2 with the smallest Mn_{PS}. For the lowest weight-average molecular weight studied, *L* is 15.9 ± 0.4 nm at $T_c = 30$°C and 17.3 ± 0.2 nm at $T_c = 40$°C, given an average increase of 25%. This behavior indicates that the chains of PS_2, with a smaller size compared with PCL, can go more easily between PCL lamellae and increasing *L*. By comparing values of *L* for the blends 20/80 PCL/PS_3 and PCL/PS_1 it can be concluded that the effect of increasing the polydispersity is the same as is observed with increasing molecular weight, that is, a decrease in the interlamellar spacing. On the other hand, in the blends containing Mn_{PS} close or higher than that of PCL, blend

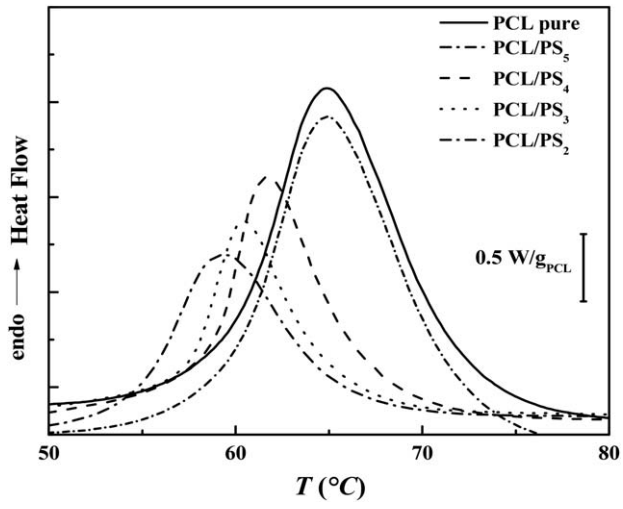

FIG. 9. Thermograms corresponding to pure PCL and 20/80 PCL/PS blends (***Series B***) isothermically crystallized at 30°C.

DOI 10.1002/pen

TABLE 9. Lamellar thickness (L) of PCL/PS_5 blends (*Series C*) at crystallization temperatures of 30°C and 40°C.

w_{PS5}	$T_c = 30$°C L (nm)	$T_c = 40$°C L (nm)
0.8	12.8 ± 0.4	13.6 ± 0.4
0.6	12.9 ± 0.3	13.7 ± 0.5
0.4	12.9 ± 0.4	13.6 ± 0.3
0.2	12.7 ± 0.4	13.5 ± 0.3

with PS_4 and PS_5, the lamellar spacing are similar to the value obtained for pure PCL at both crystallization temperatures studied (see Fig. 6), indicating that the chains of PS do not influence the spacing of PCL lamellae [14, 19]. In Fig. 8, L was plotted versus the Mn_{PS} for these blends while in Fig. 9 the thermograms corresponding to pure PCL and 20/80 PCL/PS blends (***Series B***) isothermically crystallized at 30°C are shown.

For a constant weight fraction of PS in the blends, regardless of the crystallization temperature used, the heat of fusion and the melting temperature (T_m) of PCL decrease with decreasing Mn_{PS} used (see Fig. 9). Since the values of L for blends with the lowest weight average molecular weight of PS are considerably higher than in other blends, but the crystalline fraction remains almost constant (47.9% ± 1.4% and 53.5% ± 0.7% for $T_c = 30$°C and $T_c = 40$°C, respectively, see Table 8), it is possible to conclude that L values do not correlate with an increase in the crystallinity. In Epoxy/PHB blends cured at 80°C and 120°C, by Tognana et al. [48] observed a similar behavior. While the crystalline fraction of the blends cured at 120°C was 25% and the crystalline fraction of blends cured at 80°C was 56%, values of $L = 19.8$ nm for $T_m = 120$°C, considerably higher that $L = 5.5$ nm for $T_m = 80$°C, were reported.

In Table 9 the lamellar spacing for immiscible blends PCL/PS_5, corresponding to the ***Series C***, crystallized at both temperatures is shown. Groeninckx et al. explain that the discussion on the crystallization behavior of neat polymers would be expected to be applicable to immiscible polymer blends, where the crystallization takes place within domains of nearly neat component, largely unaffected by the presence of other polymers. However, although both phases are physically separated, they can exert a profound influence on each other and the crystallization behavior can be altered by two phenomena, inherently correlated with immiscible two-phase systems, namely migration of impurities during melt-mixing and the nucleating activity of the interface between two phases [49]. In this case as constant L values were obtained, it is possible to conclude that PS_5 (with the highest Mn_{PS} value) does not affect the spacing between lamellae, which confirms the results obtained for blends with PS of different Mn_{PS} (Fig. 8). The value of L is independent of the weight fraction of PS_5 in the blend, depending only on the crystallization temperature employed. Taking into account the Mn_{PS} of the homopolymers used in the blends, PS chains involved in the crystalline phase must be in the same order of PCL. In this sense PS chains do not affect L values of PCL.

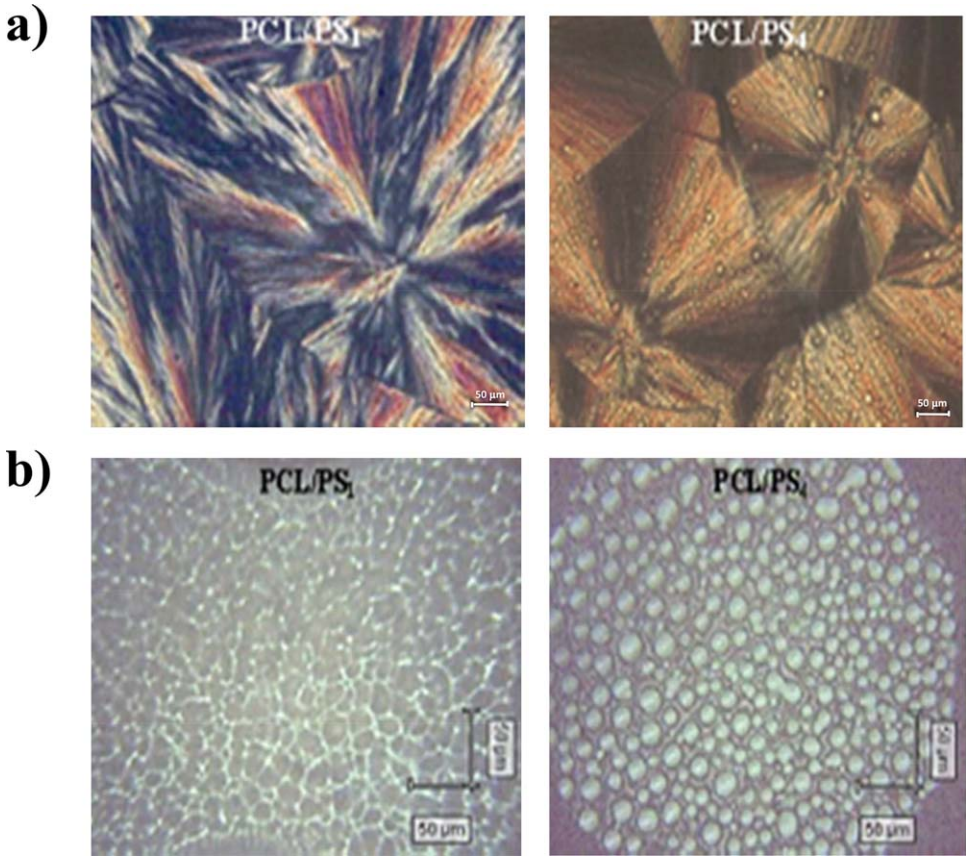

FIG. 10. Microcopies of blends 40/60 of PCL/PS_1 and PCL/PS_4 by (a) OM and (b) CRM. [Color figure can be viewed at wileyonlinelibrary.com]

In order to compare the effect of Mn_{PS} on final morphologies we studied 40/60 blends of PCL with PS_1 and PS_4 by optical (OM) and Confocal Raman microscopes (CRM). Results are shown in Fig. 10. OM microscopies in Fig. 10a display the typical spherulite morphologies of pure PCL for both blends. It can be seen in all cases, compact spherulites but does not guarantee that there are no crystallized small chains that have been rejected to interfibrillar zones. Whereas PCL/PS_1 texture shows no differences with pure PCL, for PCL/PS_4 was observed dispersed droplets over the whole spherulites surface. The phase separation excludes PS_4 chains outside the lamellae and subsequently they were piled up at the interspherulitic regions. Therefore, it is easily expected that the long period L of PCL lamellar morphology is close to that of pure PCL homopolymers with increasing the molecular weight of PS homopolymers. The displacement of the critical point shown in Fig. 3 explains the different morphologies shown in Fig. 10b: it was observed for PCL/PS_1 co-continuos morphology with spinodal decomposition while for PCL/PS4 the morphology corresponds to a binodal phase-separated system [3, 50].

CONCLUSIONS

The phase diagrams for PCL/PS were determined and it was noticed that when Mn_{PS} increases, the critical composition diminishes while its temperature increases. That is the same effect that produces the increase in the polydispersity of PS. From the fitting of phase diagrams of blends of PCL with PSO and PS, taking into account the polydispersity, two different expressions for interaction parameters were determined. As both χ have the same enthalpic contribution but the entropic ones diminishes for the PS homopolymers it is possible to conclude that the miscibility in these systems is due only by entropic effects.

Different effects of segregation morphology for polymer blends of PCL/PS were obtained as a result of change in T_c, *or* M_{nPS} and w_{PS} of amorphous component.

The crystalline fraction as well as the interlamellar spacing increased with crystallization temperature. This fact can be due to that the higher T_c approaches to the optimum crystallization temperature of pure PCL leading to a high crystal growth rate, as has been denoted with high l_c values, and a diffusion limited mobility of the amorphous component. On the other hand the highest T_c makes the interfibrillar segregation higher in pure PCL and only in the blends with lowest concentration of PS. As T_c decrease the rate of diffusion is less than the crystallization growths and the amorphous polymer can be trapped in the interfibrillar region.

The molecular weight effect was studied in blends 20/80 of PCL with PS of different molecular weight in ***Series B***: L decreases with an increase in the Mn_{PS} while the heat of fusion and the melting temperature increase. In blends with the PS of highest molecular weight studied in ***Series C*** the value of L obtained is coincident with that of pure PCL and with those obtained for the blends 20/80 made with PS_4 and PS_5 belonging to ***Series B***. We conclude that PCL lamellar morphology is not affected when the molecular weight of PS employed in the blends is similar or higher than that of PCL. As a result, high molecular weight impedes the penetration of the amorphous component into the structure lamellae making it possible to observe in the interspherulitic region using optics and confocal microscopy.

In the PCL/PS_1 (***Series A***) when increasing the w_{PS} increases the average long period (L) because the thickness of amorphous phase (l_a) is bigger. This behavior occurs till a weight fraction of 60%, for higher mass fractions L is almost constant indicating the interfibrillar segregation of PS. However, the volume fraction of PCL ($\theta_{PCL}^{a,IF}$) segregated interfibrillary not was increase by the w_{PS}. On the other hand, the thickness l_c remained constant as well as the crystalline fraction of PCL, independently of the mass fraction of PS studied.

ACKNOWLEDGMENTS

Authors want to thank to "Materials + Technologies" Group, Escuela Politécnica, Universidad País Vasco/Euskal Herriko Unibertsitatea. Donostia/San Sebastián, Spain for AFM photograph. The authors acknowledge the support of the LNLS, Brazil (Project: D11A- SAXS1- 8170)

REFERENCES

1. E. Piorkowska and G. C. Rutledge, *Handbook of Polymer Crystallization*, John Wiley & Sons, Inc. Hoboken, New Jersey (2013).
2. H. Wang, M. Langner, and S. Agarwal, *Polym. Eng. Sci.*, **56**, 1146 (2016).
3. Y. Li, M. Stein, and B.J. Jungnickel, *Colloid Polym. Sci.*, **269**, 772 (1991).
4. M.L. Di Lorenzo, P. La Pietra, M.E. Errico, M.C. Righetti, and M. Angiuli, *Polym. Eng. Sci.*, **47**, 323 (2007).
5. M.A. Woodruff and D.W. Hutmacher, *Prog. Polym. Sci.*, **35**, 1217 (2010).
6. L.A. Utracki, in *Chapter 1 of Polymer blends Handbook*, L.A. Utracki, Ed., Kluwer Academic Publishers, Dordrecht, The Netherlands (2002).
7. L.I. Atanase, O. Glaied, and G. Riess, *Polymer*, **52**, 3074 (2011).
8. G.C. Alfonso and T.P. Russell, *Macromolecules*, **19**, 1143 (1986).
9. N. López-Rodríguez, A. López-Arraiza, E. Meaurio, and J.R. Sarasua, *Polym. Eng. Sci.*, **46**, 1299 (2006).
10. M.L. Di Lorenzo, *Prog. Polym. Sci.*, **28**, 663 (2003).
11. H. Tanaka and T. Nishi, *Phys. Rev. A*, **39**, 783 (1989).
12. H.W. Kammer and C. Kummerloewe, *Polym. Eng. Sci.*, **36**, 1608 (1996).
13. S. Nojima, Y. Terashima, and T. Ashida, *Polymer*, **27**, 1007 (1986).
14. H. Shabana, R. Olley, D. Bassett, and B.J. Jungnickel, *Polymer*, **41**, 5513 (2000).
15. H. Tanaka and T. Nishi, *Phys. Rev. Lett.*, **55**, 1102 (1985).
16. T.S. Plivelic, S.N. Cassu, M.C. Gonçalves, and I.L. Torriani, *Macromolecules*, **40**, 253 (2007).
17. M. Vanneste, G. Groeninckx, and H. Reynaers, *Polymer*, **38**, 4407 (1997).
18. S. Talibuddin, L. Wu, J. Runt, and J.S. Lin, *Macromolecules*, **29**, 7527 (1996).
19. H.L. Chen, L.J. Li, and T.L. Lin, *Macromolecules*, **31**, 2255 (1998).

 DOI 10.1002/pen

20. L.A. Baldenegro Perez, D. Navarro Rodriguez, F.J. Medellin Rodriguez, B. Hsiao, C.A. Avila Orta, and I. Sics, *Polymers*, **6**, 583 (2014).
21. D. Van Krevelen and K. Nijenhuis, *Properties of Polymers*, 4th ed., Elsevier, Amsterdam (2009).
22. C. Bordes, V. Fréville, E. Ruffin, P. Marote, J.Y. Gauvrit, S. Briançon, and P. Lantéri, *Int. J. Pharm.*, **383**, 236 (2010).
23. J.D. Hoffman and J.J. Weeks, *J. Res. Natl. Bur. Stand. -a. Phys. Chem.*, **66A**, 13 (1962).
24. C.C. Riccardi, J. Borrajo, R.J.J. Williams, E. Girard-Reydet, H. Sautereau, and J.P. Pascault, *J. Polym. Sci., Polym. Phys. Ed.*, **34**, 349 (1996).
25. P.J. Flory, *Principles of Polymer Chemistry*, Cornell University Press, Ithaca, NY (1953).
26. K. Kamide, S. Matsuada, and H. Shirataki, *Eur. Polym. J.*, **26**, 379 (1990).
27. L.H. Peebles, *Molecular Weight Distributions in Polymers*, Wiley Interscience, New York (1971).
28. R. Koningsveld and A.J. Staverman, *J. Polym. Sci. Part a-2*, **6**, 325 (1968).
29. T. Nishi, T.T. Wang, and T.K. Kwei, *Macromolecules*, **8**, 227 (1975).
30. E.M. Woo, T.K. Mandal, and S.C. Lee, *Colloid Polym. Sci.*, **278**, 1032 (2000).
31. T.P. Russell, R.P. Hjelm, Jr, and P.A. Seeger, *Macromolecules*, **23**, 890 (1990).
32. L. Bonnaud, A. Bonnet, J.P. Pascault, H. Sautereau, and C.C. Riccardi, *J. Appl. Polym. Sci.*, **83**, 1385 (2002).
33. Y.P. Huang, X. Xu, X.L. Luo, and D.Z. Ma, *Chinese J. Polym. Sci.*, **20**, 45 (2002).
34. R.A. Matkar and T. Kyu, *J. Phys. Chem.*, **110**, 12728 (2006).
35. H. Xu, R. Matkar, and T. Kyu, *Phys. Rev. E*, **72**, 011804 (2005).
36. O. Glatter and O. Kratky, *Small Angle X-ray Scattering*, Academic Press Inc., London (1982).
37. G.R. Strobl and M.J. Schneider, *J. Polym. Sci. Part B: Polym. Phys. Ed.*, **18**, 1343 (1980).
38. G.R. Strobl, *The Physics of Polymers Concepts for Understanding Their Structures and Behavior*, Springer-Verlag, Berlin Heidelberg (2007).
39. R. Neppalli, V. Causin, C. Marega, R. Saini, M. Mba, and A. Marigo, *Polym. Eng. Sci.*, **51**, 1489 (2011).
40. F.L. Ji, J.L. Hu, and S. Sin-Yin Chui, *Polym. Eng. Sci.*, **52**, 1015 (2012).
41. L. Silva, S. Tognana, and W. Salgueiro, *J. Polym. Sci. Part B: Polym. Phys. Ed.*, **51**, 680 (2013).
42. P.P. Huo, P. Cebe, and M. Capel, *Macromolecules*, **26**, 4275 (1993).
43. F.B. Khambatta, F. Warner, T. Russell, and R.S. Stein, *J. Polym. Sci.Polym. Phys. Ed.*, **14**, 1391 (1976).
44. V. Crescenzi, G. Manzini, G. Calzolari, and C. Borr, *Eur. Polym. J.*, **8**, 449 (1972).
45. S. Nojima, K. Satoh, and T. Ashida, *Macromolecules*, **24**, 942 (1991).
46. G. Defieuw, G. Groeninckx, and H. Reynaers, *Polymer*, **30**, 2158 (1989).
47. Q. Guo, C. Harrats, G. Groeninckx, H. Reynaers, and M.H.J. Koch, *Polymer*, **42**, 6031 (2001).
48. S. Tognana, L. Silva, and W. Salgueiro, *Polímeros*, **23**, 358 (2013).
49. G. Groeninckx, C. Harrats, M. Vanneste, and V. Everaert, *Polymer Blends Handbook*, 2nd ed., L.A. Utracki and C.A. Wilkie, Eds., Springer, Netherlands (2014).
50. J.S. Oh, G.J. Jang, and Y.C. Bae, *Polymer*, **38**, 3761 (1997).